



1 Refining Marine Net Primary Production Estimates: Advanced
2 Uncertainty Quantification through Probability Prediction
3 Models

4 Jie Niu^{1,2†}, Mengyu Xie^{3†}, Yanqun Lu^{3*}, Liwei Sun⁴, Na Liu⁵, Han Qiu⁶, Dongdong
5 Liu^{1,2}, Chuanhao Wu⁷, Pan Wu^{1,2*}

6 ¹College of Resources and Environmental Engineering, Guizhou University, Guiyang 550025,
7 China

8 ²Key Laboratory of Karst Georesources and Environment, Ministry of Education, Guiyang
9 550025, China

10 ³Institute for Environmental and Climate Research, Jinan University, Guangzhou 510632,
11 China

12 ⁴Southern Marine Science and Engineering Guangdong Laboratory (Guangzhou),
13 Guangzhou 511458, China

14 ⁵College of Life Science and Technology, Jinan University, Guangzhou 510632, China

15 ⁶School of Natural sciences and Mathematics, University of Texas, Dallas, Richardson, TX
16 75080, USA

17 ⁷Yangtze Institute for Conservation and Development, Hohai University, Nanjing 210024,
18 China

19 *Corresponding author: Yanqun Lu, Pan Wu

20 E-mail address: Yanqunlv@163.com, pwu@gzu.edu.cn

21 † These authors contributed equally to this work and should be considered co-first authors.

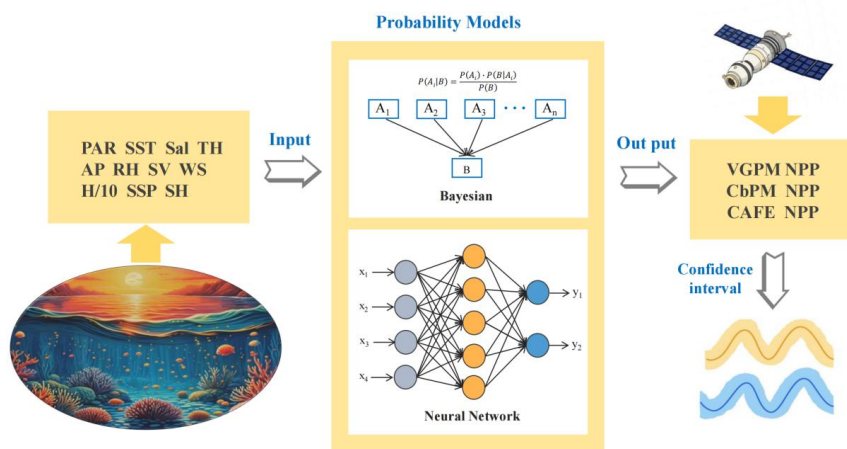
22 **Abstract**

23 In marine ecosystems, Net Primary Production (NPP) is pivotal, not merely as a
24 critical indicator of ecosystem health, but also as an integral component in the global
25 carbon cycling process. This study introduces an advanced probability prediction
26 model to refine the precision of NPP estimation and to deepen our comprehension of
27 its inherent uncertainties. A comprehensive comparative analysis is undertaken,
28 juxtaposing a Bayesian probability prediction model, predicated on empirical
29 distribution, with a probability prediction model anchored in deep learning. The
30 objective is to meticulously quantify the uncertainty associated with NPP. The
31 findings underscore the applicability of probability prediction in investigating the
32 uncertainty of marine NPP. Both models proficiently delineate the dynamic trends and
33 inherent uncertainties in NPP, with the neural network model exhibiting superior



34 accuracy and dependability. Additionally, these probability prediction models are
35 adeptly applied to prognosticate NPP in specific marine regions, efficaciously
36 elucidating the interannual trends in NPP variation. This research contributes not only
37 a more precise method for quantifying NPP uncertainty but also bolsters scientific
38 support for the stewardship of marine ecosystems and the preservation of
39 environmental integrity.

40 **Keywords:** Net Primary Production; Bayesian Probability Prediction; Neural
41 Network Probability Prediction.



42

43

graphical abstract

44 1. Introduction

45 Net Primary Production (NPP) of phytoplankton, an indispensable indicator for
46 biological productivity, exerts a substantial influence on global carbon flux and the
47 dynamics of marine ecosystems (Yang et al., 2021; Silsbe et al., 2016). The precision
48 in estimating NPP is paramount for environmental quality assessments (Falkowski et
49 al., 1998; Tan et al., 2005), effective fisheries resource management, and
50 comprehending the impacts of global climate change (Lee et al., 2015; Ding et al.,
51 2016). Conventional methods of NPP measurement, such as ship-based sampling and



52 bottle incubations, are beset with challenges like human errors and inadequacies in
53 capturing spatial and temporal dynamics. This underscores the necessity for more
54 sophisticated and comprehensive methods (Yang et al., 2021; Li et al., 2020).

55 The advent of ocean observation satellites and ocean color remote sensing
56 technology has catalyzed a paradigm shift in the estimation of large-scale marine
57 primary productivity (Yang et al., 2021; Westberry et al., 2008). These pioneering
58 technological advancements furnish novel insights into phytoplankton photosynthetic
59 production and its integral role in the carbon cycle, thereby broadening the
60 observational spectrum and establishing a robust foundation for predicting marine
61 NPP. Initial remote sensing endeavors to estimate NPP, employing satellite-based
62 chlorophyll-a (Chl-a) (Platt et al., 1991; Platt & Sathyendranath, 1988;
63 Sathyendranath et al., 1995), stemmed from the established correlation between
64 chlorophyll and photosynthesis (Ryther, 1956; Ryther & Yentsch, 1957). However,
65 these efforts were predominantly confined to local or regional applications. A
66 subsequent investigation by Campbell et al. (2002) delved into the accuracy of
67 various satellite primary productivity algorithms, unveiling that estimates from the
68 most effective algorithm often diverged from those derived from those obtained using
69 the ¹⁴C isotope labeling method. Their study also unearthed systematic biases in
70 several algorithms, which could be alleviated through re-parameterization.

71 In response to the aforementioned limitations, several remote sensing-based
72 models, such as the Vertically Generalized Production Model (VGPM), the
73 Carbon-based Productivity Model (CbPM), and the Carbon, Absorption, and
74 Fluorescence Euphotic-resolving model (CAFE), have been innovatively proposed
75 (Behrenfeld et al., 1997; Westberry et al., 2008; Silsbe et al., 2016). Spanning various
76 decades, these models address diverse facets of ocean primary production and are
77 readily accessible via satellite remote sensing data platforms. As a result, they have
78 been extensively applied and discussed in numerous studies (Westberry et al., 2008;
79 Pan et al., 2012; Dave et al., 2013; Li et al., 2020; Yang, 2021; Cael, 2021).



80 Particularly, VGPM formulates a light-dependent, depth-integrated model that
81 classifies environmental factors influencing the vertical distribution and optimal
82 assimilation efficiency of primary production, leveraging ^{14}C productivity
83 measurement data (Behrenfeld et al., 1997). Conversely, CbPM was a depth-resolved
84 spectral NPP model designed for phytoplankton growth rates (Westberry et al., 2008).
85 Its foundational concept was originally articulated by Behrenfeld et al. (2005).
86 Distinguishing itself from Chl-based models, CbPM enables the differentiation of
87 physiological changes in biomass and Chl, thus offering a more nuanced depiction of
88 phytoplankton production. Notably, its strength lies in addressing issues related to
89 light and nutrient adaptation, thereby enhancing its capability in estimating fixed
90 carbon output at the ocean surface. Similarly, the CAFE model, introduced in 2016,
91 presents an adaptive framework that melds satellite ocean color analysis with essential
92 physiological and ecological attributes of phytoplankton (Silsbe et al., 2016). It
93 incorporates intrinsic optical properties into the model and calculates NPP by
94 assessing the product of energy absorption and the efficiency of converting absorbed
95 energy into carbon biomass, alongside computing growth rates. Nonetheless, these
96 models commonly generate a single value of NPP, overlooking the range estimation
97 and the inherent uncertainties in NPP estimation, stemming either from the model
98 itself (BIPM et al., 2009) or from the model input (Milutinovic & Bertino, 2011). This
99 oversight is critical, as suggested by Saba et al. (2011), since uncertainties in input
100 variables, like Chl-a, significantly impinge upon model performance and accuracy. In
101 a recent assessment, Westberry et al. (2023) examined the daily depth-integrated NPP
102 rates over 2003–2018 for VGPM, CbPM, and CAFE, revealing that the mean NPP
103 fields of CbPM and CAFE, along with their associated frequency distributions, are
104 distinctly divergent from those of VGPM.

105 Transitioning from the constraints of traditional models, probabilistic forecasting,
106 in contrast to deterministic forecasting (Juban et al., 2007), generates a cumulative
107 distribution function or probability density function for the predicted object. This
108 methodology offers a more holistic understanding of likely outcomes (Gneiting &



109 Katzfuss, 2014; Schepen et al., 2018; Zhao et al., 2015). Significantly, this approach
110 has been successfully implemented in fields such as hydrology (Schepen et al., 2018;
111 Zhao et al., 2015; Schwanenberg et al., 2015) and power system management
112 (Al-Gabalawy et al., 2021). For instance, Schwanenberg et al. (2015) conducted
113 analyses using both deterministic and probabilistic forecasts. They concluded that
114 deterministic forecasts tend to overlook forecast uncertainty in short-term decisions,
115 whereas probabilistic forecasting offers numerous advantages: (i) it enables a longer
116 forecast horizon, facilitating earlier and more accurate predictions of major events; (ii)
117 stochastic optimization yields more robust decisions compared to deterministic
118 procedures that focus solely on individual future trajectories; and (iii) it permits
119 introduction of advanced chance constraints for refining the system operation.

120 Although Bayesian models and probabilistic neural networks are established
121 methods, their application to the remote sensing of marine net primary productivity
122 (NPP) represents a novel approach. This study leverages these advanced probabilistic
123 techniques to address the unique challenges in estimating NPP from satellite data,
124 providing a more accurate and reliable quantification of uncertainties. We introduce
125 probabilistic prediction models to meticulously quantify the uncertainty of NPP
126 estimation, thereby enhancing our comprehension of NPP's significance in marine
127 ecosystems. The research objectives of this paper are articulated as follows: (1) to
128 thoroughly quantify the uncertainty of NPP estimation through the integration of
129 probabilistic forecasting; (2) To evaluate and contrast the efficacy of neural
130 network-based probabilistic forecasting with empirical distribution-based Bayesian
131 probabilistic forecasting in capturing NPP uncertainty; and (3) To implement
132 probabilistic forecasting of the uncertainty of the NPP in the study area during
133 2007–2018 and to explore its temporal characteristics. Our study offers innovative
134 perspectives and methodologies for addressing the uncertainty associated with NPP.
135 The organization of this paper is as follows: Section 2 outlines the study area and data
136 sources; Section 3 elaborates on the methodology and presents metrics for evaluating
137 forecasting performance; Section 4 discloses the results; and Section 5 presents the



138 conclusions.

139 **2. Data and Methods**

140 **2.1. Study Area and Data Sources**

141 The research locale for this study is situated in the aquatic environs of Weizhou
142 Island, nestled within the Gulf of Tonkin, Guangxi Province, southern China (Fig. 1).
143 The proportion of excellent water quality in Guangxi's near-shore waters reaches
144 more than 90% all year round, and the quality of the marine ecological environment
145 has remained at the forefront of the country for 12 consecutive years, which is the
146 only stable habitat and feeding ground for large cetaceans known in China's
147 near-shore waters at present. Weizhou Island is the youngest volcanic island in China
148 geologically, with more than 95% of its strata comprising volcanic rocks, and
149 landscapes of sea erosion, sea accumulation, and dissolved rocks. Surrounded by the
150 sea on all sides, Weizhou Island is in the southern subtropical monsoon zone, with a
151 pleasant climate, rich heat, and abundant precipitation throughout the year. The
152 average annual temperature is 23°C, and the average winter temperature is 16.3°C.
153 The unique climatic conditions and island landscape make it a popular tourist
154 destination. The waters of Weizhou Island are the habitat of many rare marine
155 organisms, and the protection and research of its marine ecosystem are of great
156 significance to maintaining marine biodiversity.

157 The dataset of this study encompasses eight distinct sets of monitoring data
158 spanning from January 2007 to February 2018, amassing a total of 4077 days. These
159 data were procured from the Weizhou Marine Environmental Monitoring Station
160 (21.0017°N, 109.0117°E) and encompass a spectrum of variables: sea surface
161 temperature (SST), salinity (Sal), tide height (TH), air pressure (AP), relative
162 humidity (RH), sea visibility (SV), wind speed (WS), and 1/10th significant wave
163 height (H/10). Additionally, photosynthetically active radiation (PAR) was retrieved
164 from NASA's Ocean Color portal (<https://oceancolor.gsfc.nasa.gov/>), sea surface
165 precipitation (SSP) was sourced from Nasa Earth Observation Data



166 (<https://www.earthdata.nasa.gov/>), and sunshine hours (SH) was sourced from the
167 China Meteorological Administration (<https://data.cma.cn/>). This compilation resulted
168 in a comprehensive dataset comprising eleven variables. For the analysis of three NPP
169 algorithms — namely, VGPM, CbPM, and CAFE — we acquired datasets at an
170 eight-day temporal resolution from the Ocean Productivity website
171 (<http://orca.science.oregonstate.edu/npp.visual.php>). This data acquisition process
172 spanned a cumulative duration of 514 days. The specific datasets utilized for this
173 study are itemized in Table 1.

174 Due to factors such as equipment malfunctions and adverse weather conditions,
175 some data for the eleven variables were incomplete. To gain a deeper understanding
176 of the data structure and address these gaps, we conducted an analysis of the missing
177 data and identified five variables with missing entries (Table 2): SV, H/10, SSP, PAR,
178 and SH. Subsequently, we visualized these five variables in a chronological sequence,
179 with the findings depicted in Fig. 2. Distinct from daylength, which is computable
180 based on location and date, SH indeed refers to the daily measured duration of
181 sunlight reaching the Earth's surface. The variability and instances of zero values
182 observed in Fig. 2 (bottom panel) and mentioned in Table 2 reflect real-world
183 fluctuations due to weather conditions—on overcast or rainy days, actual sunshine
184 hours recorded can indeed drop to zero. These data are collected on a daily basis,
185 hence the seemingly sporadic pattern rather than a smooth temporal variation
186 expected of constant daylength calculations. The analysis revealed a marked
187 periodicity in these variables, prompting us to employ time series interpolation as our
188 method of choice for data imputation. The efficacy of this approach is evidenced in
189 Table 3, which presents the statistical indicators of the data both pre- and
190 post-interpolation. Notably, while the post-interpolation data retains a close
191 resemblance to the original data in terms of statistical indicators, it is important to
192 acknowledge that interpolated data are not independent observations. The validity of
193 the interpolation method, therefore, depends on the specific application and context.
194 In this study, interpolation was used to address missing variables, and we ensure that



195 the statistical properties of the original data were preserved to the greatest extent
196 possible. This approach allows us to maintain the integrity of our analyses while
197 recognizing the inherent limitations of using interpolated data.

198 Upon visualizing the values of the three NPP products (VGPM, CbPM, and
199 CAFE) (Fig. 3), it became evident that each exhibits a distinct periodicity, with the
200 fluctuation ranges remaining stable yet markedly varied among them. Specifically,
201 VGPM NPPs are the smallest, followed by CAFE NPPs, while CbPM NPPs have the
202 largest values. To elucidate the correlation between these NPP products and our
203 dataset, we generated Pearson correlation plots (Fig. 4). The results revealed that the
204 variables with the highest correlations differed among the three NPP values. Notably,
205 VGPM NPP showed the strongest correlation with SST, because the estimation of
206 VGPM NPP is directly dependent on the optimal assimilation efficiency of the
207 productivity profile (Behrenfeld et al., 1997). Whereas both CAFE NPP and CbPM
208 NPP were most closely correlated with AP, albeit in opposing directions—CAFE NPP
209 displayed a positive correlation and CbPM NPP, a negative one. Changes in AP
210 mainly affect atmospheric stability, cloudiness, and precipitation, which in turn
211 indirectly affect light conditions in the ocean and phytoplankton photosynthesis.
212 Photosynthesis in plants may be inhibited under low-pressure environments. This
213 analysis highlights that the three NPP estimation models exhibit distinct affinities with
214 each variable. In summary, among the three models, VGPM NPP possesses the most
215 significant correlation with the variables, followed by CAFE NPP, and lastly CbPM
216 NPP.

217 2.2. Methods

218 2.2.1. Bayesian Probability Prediction

219 Bayesian models can adeptly quantify the uncertainty in the distribution of
220 predicted outcomes. The Bayesian approach is particularly advantageous in scenarios
221 with limited training data or when potential invisibility in training data cannot be



222 discounted in practical applications (Perfors et al, 2011). The Bayesian formula is
223 represented as:

$$P(\theta|D) = \frac{P(D|\theta) \cdot P(\theta)}{P(D)} \#(1)$$

224 where $P(\theta|D)$ denotes the posterior probability, $P(D|\theta)$ the likelihood probability,
225 $P(\theta)$ the prior probability, and $P(D)$ the marginal probability for normalization.

226 When a training dataset D is available, the probability distribution $P(\theta|D)$ of θ is
227 computable using the aforementioned Bayesian formula (Dürr et al, 2020). To deduce
228 $P(\theta|D)$, it is imperative to ascertain the likelihood probability $P(D|\theta)$ of the observed
229 data under the model parameter θ . $P(D|\theta)$ can also be interpreted as the probability of
230 obtaining the training dataset D given parameter θ . Additionally, knowledge of the
231 prior probability $P(\theta)$ and the evidence $P(D)$ is essential. Given that the training
232 dataset D is fixed, $P(D)$ remains constant. Consequently, the posterior distribution is
233 proportional to the likelihood probability multiplied by the prior distribution, i.e.,
234 $P(\theta|D) \propto P(D|\theta) \cdot P(\theta)$, in accordance with Bayes' Law.

235 In this study, the Bayesian approach is employed to calculate the posterior
236 distributions of the parameters considering the prior information and the input data.
237 Subsequent predictions are made using the posterior distributions, yielding a
238 probability distribution for each predicted value. Ultimately, the model's ability to
239 estimate the uncertainty in the NPP is illustrated by plotting the prediction ranges for
240 different targets and comparing them to actual observations.

241 2.2.2. Neural Network Probabilistic Prediction Model Based on TFP

242 TensorFlow Probability (TFP) represents a sophisticated library of statistical
243 algorithms, devised atop the TensorFlow Python API. Its primary objective is to
244 streamline the integration of probabilistic models with deep learning frameworks. TFP
245 offers a comprehensive suite of tools, enabling the construction of probabilistic



246 models adept at estimating uncertainty. Aiming to thoroughly assess the predictive
247 efficacy of the three NPP products, we employed a neural network model grounded in
248 the TFP framework, capitalizing on its versatility and potent expressive capabilities
249 for probabilistic prediction in marine ecosystems.

250 The architecture of this neural network model incorporates multiple hidden
251 layers, each implementing a nonlinear transformation via an activation function. Such
252 a configuration enables the model to automatically extract higher-order features and
253 intricate patterns from the data. Our selection of TFP as the implementation medium
254 allows us to model the neural network's output by integrating probability distributions,
255 thus addressing the model's uncertainty regarding predictions and yielding more
256 exhaustive insights. Specifically, our neural network model utilizes a distribution
257 layer in the output stage, producing a probabilistic distribution concerning the target
258 variable, as opposed to a mere deterministic point prediction. This probabilistic output
259 facilitates the quantification of the model's confidence level for each prediction,
260 extending beyond mere point estimates.

261 The integration of Bayesian models and probabilistic neural networks in our
262 approach addresses key challenges in the remote sensing of NPP. These challenges
263 include handling the variability and uncertainty inherent in satellite-derived data and
264 environmental factors, thus improving the robustness of NPP estimates. In this study,
265 the input variables for the models are the 11 environmental variables mentioned in
266 Section 2.1, and the outputs are VGPM, CbPM, and CAFE NPPs. The selection of
267 input data was not limited to variables directly related to phytoplankton
268 photosynthesis, such as SST, PAR, and SH. Instead, it also included a wide range of
269 environmental variables that could influence phytoplankton growth, such as TH, WS,
270 and AP, which are physical dynamics and meteorological characteristics. Since
271 phytoplankton are the primary source of NPP, environmental factors affecting
272 phytoplankton growth also indirectly impact NPP. The dataset spans 4,077 days, but
273 due to the 8-day time interval of the downloaded NPP products, only 514 complete



274 datasets are available for model training and performance evaluation. Given the
275 limited amount of data, 80% of the 514 sets are used for model training and parameter
276 tuning, while the remaining 20% are used for performance evaluation. In the neural
277 network probabilistic prediction model, there are six layers, with two output nodes
278 used to estimate the mean and standard deviation. The Gaussian distribution is
279 employed in the distribution layer, and the loss function is the negative log-likelihood
280 loss function. The detailed parameters of the neural network are presented in Table 4.

281 2.3. Model Evaluation

282 Prior to model evaluation, we normalized the NPP satellite data. This step is
283 critical to improving model performance because it removes the potential effects of
284 different data scales, allowing the model to consider each data point more fairly.
285 Normalization ensures that the distribution range of NPP data has the same weight
286 during model training, thus improving the model's ability to capture the inherent
287 patterns and features of the data. In addition, normalization helps reduce the noise and
288 bias introduced by data scale differences, further enhancing the stability and
289 predictive accuracy of the model.

290 Before training the model, we divided the dataset reasonably. Specifically, we
291 divided the dataset into 80% training set and 20% testing set. This division aims to
292 ensure that the model can fully learn the features and patterns of the data during the
293 training process, while retaining enough independent data for testing the predictive
294 ability of the model. This way of dividing the dataset helps us to evaluate the
295 performance of the model more accurately and avoid problems such as overfitting.

296 2.3.1. CRPS

297 Continuous Ranked Probability Score (CRPS) is a sophisticated statistical metric
298 employed to evaluate the efficacy of forecasting models. Initially introduced in the
299 1970s (Matheson & Winkler, 1976), CRPS is widely utilized in areas such as weather



300 forecasting (Zamo et al., 2018). It quantifies the divergence between the predicted
301 probability distribution and the actual observations (Hersbach, 2000). Ideally suited
302 for scenarios where the target variable is continuous and the model predicts its
303 distribution (Pic et al., 2023), CRPS equates to the mean absolute error (MAE) in
304 deterministic forecasting (Zhao et al., 2015).

305 In probabilistic forecasting, the focus extends beyond mere point estimates to
306 encompass the shape and dispersion of the probability distribution. Hence, traditional
307 scoring functions prove inadequate, as aggregating the predicted distributions into
308 their mean or median neglects critical information about the dispersion and shape.
309 CRPS, by embracing the entire probability distribution, emerges as an invaluable tool
310 in assessing model uncertainty. CRPS is calculated as follows:

311 1. For each sample, calculate the discrepancy between the cumulative
312 distribution function (CDF) of the predicted and observed values.

313 2. Aggregate the variances for all samples and divide by the number of samples
314 to obtain the average variance.

$$315 \quad CRPS(F, x) = \int_{-\infty}^{+\infty} [(F(y) - H(y - x))]^2 dy \quad (2)$$

$$316 \quad CRPS = \frac{1}{n} \sum_{i=1}^n CRPS(F_i, x_i) \quad (3)$$

317 where $F(y)$ denotes the CDF of the predicted value, y the predicted value, x the
318 observed value, and $H(y-x)$ the Heaviside function which is 0 when $y < x$ and 1
319 otherwise. n indicates the total number of samples, and $CRPS(F_i, x_i)$ the CRPS value
320 for the i -th sample.

321 A smaller CRPS value signifies a closer alignment of the model's probability
322 distribution with actual observation, integrating insights on both the shape and
323 location of the distribution and demonstrating sensitivity to outliers. Unlike other



324 metrics such as Root Mean Square Error (RMSE) or Mean Absolute Error (MAE),
325 CRPS offers a more holistic evaluation of a probability distribution's predictive
326 capacity by considering the full distribution shape. For Bayesian and neural network
327 models, comparing CRPS values facilitates an understanding of their proficiency in
328 fitting the entire probability distribution.

329 2.3.2. RMSD

330 Root Mean Squared Deviation (RMSD) is a widely recognized evaluation metric
331 in regression analyses, primarily employed to quantify the discrepancy between a
332 model's predicted values and the actual observed values. Characterized by its intuitive
333 nature and simplicity in computation, RMSD is particularly beneficial in scenarios
334 where emphasis is placed on the magnitude of difference between predicted and
335 actual values, irrespective of the difference's direction.

$$336 \quad \text{RMSD} = \sqrt{\frac{1}{n} \sum_{i=1}^n (y_i - \hat{y}_i)^2} \quad (4)$$

337 where n denotes the number of samples, y_i represents the actual value of the i -th
338 sample, and \hat{y}_i symbolizes the predicted value of the i -th sample.

339 A lower RMSD value is indicative of superior model performance, signaling a
340 smaller variance between the model's predictions and the observed values.
341 Nevertheless, it is important to note that RMSD exhibits sensitivity to outliers, as it
342 constitutes the mean of the squared differences. Incorporating RMSD alongside CRPS
343 in our analysis enables a more comprehensive evaluation of both the overall accuracy
344 and uncertainty inherent in the predictions.

345 2.3.3. MAPD

346 Mean Absolute Percentage Deviation (MAPD) is a frequently utilized percentage
347 error metric in regression problems. It expresses the prediction error as a percentage,
348 offering an insightful perspective into the relative error between predicted results and



349 true values in predictive model evaluations.

350
$$MAPD = \frac{1}{n} \sum_{i=1}^n \left| \frac{\hat{y}_i - y_i}{y_i} \right| \times 100\% \quad (5)$$

351 where n signifies the number of samples, y_i the actual value of the i -th sample, and \hat{y}_i
352 the predicted value of the i -th sample.

353 A lower MAPD value is desirable, indicating a reduced relative error of the
354 model. However, a cautionary note: MAPD may prove unreliable in instances where
355 the predicted value approaches zero, as a zero denominator results in infinity.
356 Therefore, careful consideration is warranted when employing MAPD, particularly in
357 scenarios where relative accuracy is paramount.

358 In the context of comparing Bayesian probabilistic prediction models with neural
359 network probabilistic prediction models, the synergistic application of these three
360 metrics — CRPS, RMSD, and MAPD — affords a multifaceted assessment of the
361 models. This triad of metrics enhances our understanding of the importance of relative
362 error alongside the accuracy of point estimates and the fit of probability distributions.

363 **3. Results and Discussion**

364 **3.1. Comparative Analysis of Prediction Efficacy Between Two Models**

365 We utilized VGPM, CbPM, and CAFE NPPs as prediction targets to scrutinize
366 the predictive effectiveness of both the neural network-based probabilistic prediction
367 model and the empirical distribution-based Bayesian probabilistic prediction model.
368 Fig. 5 presents a comparison of CRPS, RMSD, and MAPD values for these models
369 across training and test datasets. Notably, CRPS provides a holistic evaluation of
370 prediction accuracy and reliability. All the metrics are calculated using normalized
371 data for better comparison. Lower values are indicative of enhanced model
372 performance. Fig. 5(a)-(c) and (d)-(f) respectively depict the CRPS, RMSD, and
373 MAPD of the NN model and Bayes model when using the three NPP values as



374 prediction targets. The color blue represents the training set, while red represents the
375 test set. It can be observed from Fig.5 (a) and (d) that the CRPS values of both the NN
376 model and Bayes model are similar. When VGPM NPP is used as a prediction target,
377 the performance of the models is closest between the training set and test set,
378 followed by CbPM NPP. However, CAFE NPP has the lowest CRPS value among all
379 three models, with its test set slightly larger than that of its training set.

380 In terms of RMSD metrics (Fig. 5 (b) and (e)), when VGPM NPP is used as a
381 prediction target, its index value is significantly higher compared to others; however,
382 its performance between training set and test set remains close. When CbPM NPP is
383 used as a prediction target, Bayes model outperforms NN model but exhibits a larger
384 difference between training set and test set compared to NN model.

385 On using CAFE NPP as a prediction target, both models show more consistent
386 performance. The values of these indicators are relatively close in all aspects at
387 around 0.2. Regarding MAPD metrics (Fig.5 (c) and (f)), clear differences among the
388 three NPP models can be seen where CAFE has obviously lower index value
389 compared to CbPM and VGPM. In addition, for NN model's MAPD index value for
390 CAFE is lower than that for Bayes model. However there exists significant difference
391 between its training set and test set.

392 Overall evaluation indicates that under both models' assessment criteria, CAFE
393 NPP demonstrates superior accuracy in predicting effects compared to VGPM NPP
394 and CbPM NPP. VGPM NPP shows greater instability with inferiority in its training
395 process over testing process (Fig.5 (d), (e), (f)), which may be attributed to overfitting.
396 However, there is a more noticeable difference in the performance of CbPM NPP in
397 the two models. The CRPS value and RMSD value in the Bayes model are
398 significantly lower than those in the NN model (Bayes is less than 0.2, while NN is
399 more than 0.2). Therefore, the following analyses will focus on the efficacy of
400 probabilistic prediction models with CAFE NPP as the prediction target.



401 3.2. Quantify the Uncertainty of CAFE NPP

402 When quantifying uncertainty in the CAFE NPP, we need to focus on the
403 uncertainty factors that exist in the input variables in addition to the uncertainty that
404 may arise during model training. These uncertainty factors include measurement
405 errors and temporal variability, among others. Measurement errors usually originate
406 from the accuracy limitations of the instruments, the complexity of the observation
407 environment, or the instability of human operations. These errors not only affect the
408 accuracy of the input variables to varying degrees, but also propagate through the
409 model and thus affect the accuracy of the prediction results. The temporal variability,
410 on the other hand, reflects the dynamic changes of marine environmental parameters,
411 such as seasonal temperature changes, cyclic fluctuations of tides, etc., which also
412 affect the NPP prediction results. Consequently, quantifying these uncertainties is
413 particularly important in conducting CAFE NPP predictions.

414 3.2.1. Comparative Analysis of Confidence Interval Widths

415 Fig. 6 illustrates the comparison between the forecast mean of the NN model and
416 Bayes model, and the CAFE NPP value when CAFE NPP is utilized as the prediction
417 target. In the figure, the triangular icons represent 514 sets of the forecast average,
418 while the gray and blue represent the 95% and 75% confidence intervals, respectively.
419 Overall, both models exhibit relatively wide confidence intervals for their predicted
420 results, possibly due to the large range of changes in CAFE NPP. The models may
421 face greater challenges in capturing this wide range of changes, resulting in increased
422 uncertainty.

423 When CAFE NPP is less than $450 \text{ mg C m}^{-2} \text{ d}^{-1}$, both models tend to
424 overestimate the actual NPP value. This phenomenon becomes more pronounced
425 when CAFE NPP is less than $350 \text{ mg C m}^{-2} \text{ d}^{-1}$. In contrast, a certain linear
426 relationship between true value and predicted mean value emerges within a range of
427 $450\text{-}600 \text{ mg C m}^{-2} \text{ d}^{-1}$. Most of the predicted mean values are distributed around the
428 1:1 line in this range, indicating higher accuracy by these models. However, when



429 CAFE NPP exceeds $600 \text{ mg C m}^{-2} \text{ d}^{-1}$, it is observed that both models tend to
430 underestimate actual NPP values. This phenomenon may be attributed to an imbalance
431 in sample data distribution within different intervals of CAFE NPP. The majority of
432 data points are concentrated in a narrow range ($350\text{-}600 \text{ mg C m}^{-2} \text{ d}^{-1}$), while data
433 points in other intervals are scarce. This inadequacy makes it difficult for model
434 training to capture its distribution law accurately and leads to increased prediction
435 uncertainty within these ranges.

436 Compared with the two models, the predicted value of NN model is more
437 concentrated around the 1:1 line, while the predicted value of Bayes model is
438 relatively dispersed and the confidence interval is wider. The smaller the confidence
439 interval width, the higher the accuracy of model prediction. It manifests that the NN
440 probabilistic prediction model is more accurate in predicting CAFE NPP than the
441 Bayes probabilistic prediction model, and the uncertainty of its prediction results is
442 lower. The prediction mean obtained by the NN probabilistic prediction model is
443 closer to the 1:1 line, which usually means that the deviation between the predicted
444 value of the model and the actual observed value is small, that is, the prediction
445 accuracy of the model is higher. The differences in the performance of the two models
446 may stem from their different strategies for dealing with uncertainty and data fitting.
447 Neural network models typically capture the nonlinear relationships of data through a
448 large number of parameters and complex network structures, so they may be able to
449 fit the data distribution more accurately in some cases. Bayes model deals with
450 uncertainty by introducing prior knowledge and a posteriori inference, but its
451 performance may be limited under some complex data distributions.

452 To further elucidate the models' effectiveness in probabilistic prediction of
453 CAFE NPP, Fig. 7 visualizes the time series model predictions with a 95% confidence
454 interval uncertainty range. The figure shows that almost all CAFE NPP values fall
455 within the 95% confidence interval of the mean of the predicted values. It can be
456 clearly seen that the predicted distribution of the NN model is much smaller than that
457 of the Bayes model, which is consistent with the results shown in Fig. 6. The NPP is



458 clearly periodic in time, and both models are able to align their predictions on the test
459 set with the periodicity of the training set. In particular, the scatter in the NN model is
460 more centrally distributed around the red line, while the scatter in the Bayes model is
461 more discrete from the red line, which further suggests that the NN model has a more
462 accurate estimate in predicting the CAFE NPP.

463 Overall, the trends in the predicted means of the two models are consistent with
464 the trends in the majority of CAFE NPP values, which further validates the accuracy
465 of the two methods in capturing the process of CAFE NPP changes. This consistency
466 not only indicates that the models can accurately reflect the long-term trends of CAFE
467 NPP changes, but also capture short-term fluctuations and outliers. This is of great
468 significance for ecosystem monitoring and prediction, and helps to better understand
469 the dynamics of the ecosystem and take appropriate management and conservation
470 measures. However, in terms of confidence interval width, the width of the 95%
471 confidence interval in the results of the Bayesian probabilistic prediction model is
472 larger than that of the neural network probabilistic prediction model, indicating that
473 the Bayesian probabilistic prediction model is not as sharp as the neural network
474 probabilistic prediction model, which is more locally sensitive and able to respond to
475 the changes in data more quickly.

476 Although the neural network probabilistic prediction model shows an advantage
477 in terms of sharpness and local sensitivity, this does not mean that it is superior to the
478 Bayesian model in all cases. In fact, Bayesian models are more robust and
479 explanatory by introducing prior knowledge and posterior inferences to deal with
480 uncertainty. Therefore, when choosing a predictive model, trade-offs need to be made
481 based on specific application scenarios and data characteristics.

482 3.2.2. Comparative Analysis of CDF

483 Evaluating the empirical CDF of the model input data and the average predictive
484 CDF affords a graphical representation of the model's predictive accuracy. A higher
485 degree of overlap in the CDF curves signifies greater similarity between the two
486 distributions, thereby reflecting superior model predictions. Fig. 8 depicts the overall



487 predictive distribution versus the empirical distribution of the CAFE NPP input data.
488 Concurrently, Fig. 9 methodically quantifies the disparity between the average
489 predictive CDF and the empirical CDF of the input data. Optimally, the divergence
490 between these two CDFs should be minimal, manifested as extensive overlap between
491 the yellow and blue curves in Fig. 8, and the blue curve in Fig. 9 approaching zero.
492 Fig. 8 demonstrates the CDF curves of the predicted mean values after the
493 normalization process and the CDF curves of the CAFE NPP. The CDF plots of the
494 normalized data can reflect the statistical distribution of the datasets, especially when
495 the different datasets have different magnitudes or scales, and the normalization can
496 eliminate these differences, which makes the comparisons and analyses between the
497 different datasets more accurate and intuitive. Fig. 9 specifically quantifies the
498 difference between the two CDF curves in FIG. 8 at each point, which is
499 accomplished by calculating the difference between the y-values of the two CDF
500 curves at the same x-value.

501 Observing the results in the figure, it is found that the mean values of the
502 prediction results of the NN probabilistic prediction model and the Bayes probabilistic
503 prediction model are roughly consistent with the trend of the CDF of the input
504 prediction target CAFE NPP. For the NN probabilistic prediction model, when the
505 CAFE NPP is small, the two CDF curves on the training set and the test set move
506 gently and almost overlap, with the difference close to 0, which indicates that the
507 model can predict the actual data distribution well within the range of small values of
508 CAFE NPP. As CAFE NPP increases, the difference between the CDF curves starts to
509 become larger, and the predicted mean CDF on the training set lies below the CAFE
510 NPP CDF, with the difference between the two ranging from 0 - 0.2. The predicted
511 mean CDF on the test set first lies below the true value CDF curve, and then becomes
512 steeper and lies above the true value CDF curve, and when CAFE NPP continues to
513 increase, the two curves alternate again, which may imply that the model is more
514 unstable in predicting high values, and the absolute value of the difference between
515 the CDF does not exceed 0.1.



516 For the Bayesian probabilistic prediction model, the predicted mean CDF curve
517 is above the true value in the training set. When the CAFE NPP increases to a certain
518 extent, the two curves alternate, and the absolute value of the difference between the
519 CDF does not exceed 0.2. In the test set, the two CDF curves overlap first and then
520 separate. The predicted mean CDF rises more quickly, and is on top of the true value
521 CDF curve, with the difference between the two curves not exceeding 0.1 when the
522 CAFE NPP increases to a certain extent. When the NPP increases to a certain degree,
523 the two curves overlap again, and the absolute value of the difference between the
524 CDF does not exceed 0.3. Overall, the difference between that of the predicted mean
525 values and the CDF of the true values obtained by the two models is small, which
526 indicates that the overall deviation of the model predictions is not large, and both
527 models show good prediction performance and can capture the statistical
528 characteristics of the data well. However, the CDF curves of the neural network
529 probabilistic prediction model are closer to the true values on both the training and
530 test sets, possibly implying that the neural network model is more effective in dealing
531 with complex data and capturing nonlinear relationships. The flexibility of neural
532 networks allows them to adapt to different data distributions and patterns.

533 Table 5 presents RMSD, MAPD, and CRPS for both models. Additionally, we
534 analyzed the proportion of raw input data encompassed within the 95% confidence
535 interval, thereby providing a more nuanced evaluation of the model's proficiency in
536 capturing CAFE NPP uncertainty. According to Table 5, the neural network-based
537 probabilistic prediction model exhibits superior performance in terms of CRPS,
538 RMSD, and MAPD. This denotes a higher level of accuracy and reliability for the
539 neural network model in probabilistic predictions of CAFE NPP, especially when
540 considering uncertainty. Conversely, the Bayesian probabilistic prediction model
541 demonstrates a stronger ability to encompass a greater proportion of the raw input
542 data within the 95% confidence interval. This suggests that while it may exhibit
543 higher overall uncertainty, it has a more pronounced capability to capture the nuances
544 of uncertainty.



545 This comparative analysis elucidates that both the neural network-based
546 probabilistic prediction model and the Bayesian probabilistic prediction model,
547 grounded in empirical distributions, are adept at capturing and quantifying the
548 uncertainty of CAFE NPP. While the Bayesian model demonstrates a heightened
549 capability in encompassing a broader scope of uncertainty, the neural network model
550 distinguishes itself by its superior accuracy and reliability, particularly in precisely
551 predicting the uncertainty of CAFE NPP. A notable observation is that when CAFE
552 NPP values exceed $350 \text{ mg C m}^{-2} \text{ d}^{-1}$, the predictive performance of both models
553 deteriorates. This manifests as an underestimation of mean predictions, indicating an
554 inability to fully and accurately predict NPP across the entire range of size classes.
555 The underlying reason for this may stem from the considerable variation in the input
556 data and its skewed sample distribution. Most notably, a significant proportion of the
557 samples were primarily concentrated within the $200\text{-}350 \text{ mg C m}^{-2} \text{ d}^{-1}$ range. In
558 contrast, CAFE NPP values exceeding $350 \text{ mg C m}^{-2} \text{ d}^{-1}$ constitute only 28% of the
559 input dataset. Consequently, the models exhibit insufficient learning of higher value
560 ranges during the training phase, resulting in a notable prediction bias for larger
561 CAFE NPP values.

562 3.3. Probabilistic Prediction of NPP in Weizhou Island (2007–2018)

563 Given the 8-day temporal resolution of data acquired by remote sensing satellites
564 and the consequent data incompleteness, this study employed the previously trained
565 neural network and the Bayesian probabilistic prediction models to forecast the daily
566 NPP in the Weizhou Island sea area from 2007 to March 2018, thereby supplementing
567 the NPP dataset. The results are illustrated in Fig. 10, where the predicted mean
568 values and 95% confidence intervals for both models are displayed. Fig. 10(c) reveals
569 that the Bayesian model's confidence interval is broader, primarily due to its lower
570 limit, yet no substantial difference is noted between the predicted mean values of the
571 two models. Both models effectively mirror the trend of NPP. The analysis of the
572 annual change of NPP shows a clear periodicity, which means that the change of NPP



573 is not random, but follows certain laws and patterns. Combined with Fig. 11, the
574 seasonal variation of NPP throughout the year emerges. Specifically, NPP shows a
575 decreasing trend from January to July each year, with July generally being the lowest
576 level of the whole year. Then it increases from July to November and slightly
577 decreases from November to December. Overall, NPP has larger values in winter and
578 spring. These results provide important insights into seasonal variations and
579 interannual trends of NPP in the Weizhou Island waters and provide valuable data to
580 support the study of the marine ecosystem dynamics.

581 However, the significance of our work extends far beyond mere data replication.
582 The primary aim of our study is to enhance the reliability of marine NPP estimates by
583 using advanced probabilistic models. Our objective extends beyond merely
584 reproducing satellite NPP products. We aim to improve the overall accuracy and
585 uncertainty quantification of NPP estimates by incorporating a robust probabilistic
586 framework. This framework helps to better understand and quantify the uncertainties
587 inherent in marine NPP, whether they originate from satellite data or environmental
588 factors. By using Bayesian models and probabilistic neural networks, we not only
589 replicate satellite NPP estimates but also capture and quantify uncertainties at multiple
590 levels. These models account for uncertainties in the satellite products, input data
591 variability, and the predictive model itself, thus providing a more comprehensive
592 uncertainty quantification relevant to marine NPP.

593 **4. Conclusion**

594 This study primarily addresses the challenge of uncertainty in satellite ocean
595 color data estimates of ocean NPP. Departing from traditional point estimation
596 regression models, we embraced a probabilistic prediction approach where the output
597 is a probability distribution. The models utilized in this study include a Bayesian
598 probabilistic prediction model based on empirical distributions and a deep
599 learning-based probabilistic prediction model under the TFP framework. Focusing on
600 the NPP uncertainty analysis in the Weizhou Island sea area, we explored the effect of



601 the probabilistic prediction model when the NPPs obtained by the VGPM, CbPM, and
602 CAFE methods, respectively, are used as the prediction targets. Furthermore, this
603 study compares and analyzes the capabilities of Bayesian and neural network
604 probabilistic models in predicting the CAFE NPP uncertainty. The results reveal that
605 both models are competent in quantifying CAFE NPP uncertainty.

606 When exploring the uncertainty of the NPP using the Bayesian probabilistic
607 prediction model and the neural network probabilistic prediction model, the results
608 show that the two probabilistic prediction models are the most effective when the
609 prediction target is the CAFE NPP. The probability distributions obtained by the two
610 probabilistic prediction models are similar to those of CAFE NPP, with the difference
611 in CDF between the predicted mean and true values at each data point not exceeding
612 0.2 for the neural network probabilistic prediction model and 0.3 for the Bayesian
613 probabilistic prediction model. In contrast, the confidence intervals for the outputs of
614 the Bayesian probabilistic prediction model are wider, and the proportion of the
615 CAFE NPP that falls in the confidence intervals is higher, which shows that Bayes is
616 more capable of capturing uncertainty, but its accuracy is not high. However, the
617 neural network probabilistic prediction model is more accurate and reliable. Its
618 performance is better in many assessment indicators, but not all CAFE NPP values in
619 the size range can be predicted accurately by the model. When the CAFE NPP is less
620 than $450 \text{ mg C m}^{-2} \text{ d}^{-1}$, the model tends to overestimate the actual NPP value. When
621 CAFE NPP is larger than $600 \text{ mg C m}^{-2} \text{ d}^{-1}$, it tends to underestimate the actual NPP
622 value. When the two probabilistic prediction models are applied to the prediction of
623 CAFE NPP in the Weizhou Island waters between January 2007 and February 2018,
624 the prediction results illustrate the interannual trend of CAFE NPP, and the magnitude
625 of NPP is found to show obvious cyclic changes. Our study demonstrates the novel
626 application of advanced probabilistic models to the remote sensing of marine NPP. By
627 addressing the uncertainties in satellite-derived estimates and improving the reliability
628 of NPP predictions, our work contributes to advancing the field of marine remote
629 sensing and provides a foundation for future research.



630 In the context of ongoing climate change, accurately capturing and reducing the
631 uncertainty of marine NPP emerges as a pivotal research focus in marine ecology.
632 This endeavor is crucial for a deeper understanding of energy and matter flow in
633 marine ecosystems, providing a solid scientific foundation for the judicious
634 management of the conservation of natural resources. While our study has advanced
635 the field by demonstrating the feasibility of probabilistic prediction in quantifying
636 NPP uncertainty, we acknowledge the potential for further enhancements and
637 expansions. Looking ahead, future research could embark on the following paths to
638 augment our work: (1) Expanding the research scope: The current study has
639 concentrated primarily on specific marine areas. Future initiatives could broaden this
640 focus to encompass diverse geographic regions and types of marine ecosystems. Such
641 expansion is vital to gain a more comprehensive understanding of probabilistic
642 prediction's applicability and effectiveness across varying environmental conditions;
643 (2) Enhancing data collection: The acquisition of more extensive and comprehensive
644 observational data is instrumental in refining model training and prediction accuracy.
645 Future endeavors should aim to amass a richer array of observational data,
646 emphasizing the need for long-term time series and high-resolution remote sensing
647 data. These efforts will significantly bolster the development and validation of robust
648 probabilistic prediction models; (3) Refining model structure: Our study utilized
649 Bayesian probabilistic regression and deep learning-based probabilistic prediction
650 models. Future studies could explore the integration of other advanced model
651 structures or the optimization of the existing ones, aiming to elevate the model's
652 performance and robustness. Through these concerted efforts, we aspire to continually
653 refine the methodologies of probabilistic prediction in quantifying marine NPP
654 uncertainty, thereby laying the groundwork for more precise ecosystem management
655 and environmental protection strategies.

656 **Author contribution Statement**

657 Jie Niu: Conceptualization, Methodology, Data Curation, Writing - Review & Editing,



658 Supervision, Funding acquisition.
659 Mengyu Xie: Conceptualization, Methodology, Data Curation, Writing - Original
660 Draft, Visualization.
661 Yanqun Lu: Conceptualization, Methodology, Data Curation, Writing - Original Draft,
662 Visualization.
663 Liwei Sun: Data Curation, Supervision, Funding acquisition.
664 Na Liu: Writing - Review & Editing, Supervision.
665 Han Qiu: Writing - Review & Editing, Supervision.
666 Dongdong Liu: Writing - Review & Editing, Supervision.
667 Chuanhao Wu: Writing - Review & Editing, Supervision.
668 Pan Wu: Writing - Review & Editing, Supervision.

669 **Declaration of interests**

670 The authors declare that they have no known competing financial interests or personal
671 relationships that could have appeared to influence the work reported in this paper.

672 **Acknowledgements**

673 This research was funded by the National Natural Science Foundation of China
674 [41972244], the Project of Science and Technology Department of Guizhou Province
675 (the technical system of prevention and control to mine groundwater pollution in karst
676 areas, 2022), and the High-Level Talent Training Program in Guizhou Province
677 (GCC[2023]045). Co-author Liwei Sun was partially supported by GuangDong Basic
678 and Applied Basic Research Foundation (2022A1515010590).

679 **References**

- 680 Al-Gabalawy, M., Hosny, N. S., & Adly, A. R. (2021). Probabilistic forecasting for energy time series
681 considering uncertainties based on deep learning algorithms. *Electric Power Systems*
682 *Research*, 196, 107216.
- 683 Behrenfeld, M. J., & Falkowski, P. G. (1997). Photosynthetic rates derived from satellite-based
684 chlorophyll concentration. *Limnology and oceanography*, 42(1), 1-20.
- 685 Behrenfeld, M. J., Boss, E., Siegel, D. A., & Shea, D. M. (2005). Carbon-based ocean productivity and
686 phytoplankton physiology from space. *Global biogeochemical cycles*, 19(1).
- 687 BIPM, I., IFCC, I., ISO, I., & IUPAP, O. (2009). Evaluation of measurement data an introduction to
688 the 'Guide to the expression of uncertainty in measurement' and related documents. *JCGM*, 104,
689 1-104.



- 690 Cael, B. B. (2021). Variability-based constraint on ocean primary production models. *Limnology and*
691 *Oceanography Letters*, 6(5), 262-269.
- 692 Campbell, J., Antoine, D., Armstrong, R., Arrigo, K., Balch, W., Barber, R., ... & Yoder, J. (2002).
693 Comparison of algorithms for estimating ocean primary production from surface chlorophyll,
694 temperature, and irradiance. *Global biogeochemical cycles*, 16(3), 9-1.
- 695 Dave, A. C., & Lozier, M. S. (2013). Examining the global record of interannual variability in
696 stratification and marine productivity in the low-latitude and mid-latitude ocean. *Journal of*
697 *Geophysical Research: Oceans*, 118(6), 3114-3127.
- 698 Ding, Q. X., Chen, W. Z. (2016). Spatial and Temporal Variations in Net Primary Productivity in the
699 China Seas Based on VGPM. *Marine Development and Management*, 8, 31-35.
- 700 Dürr, O., Sick, B., & Murina, E. (2020). Probabilistic deep learning: With python, keras and tensorflow
701 probability. Manning Publications.
- 702 Falkowski, P. G., Barber, R. T., Smetacek, V. (1998). Biogeochemical Controls and Feedbacks on
703 Ocean Primary Production. *Chemistry and biology of the oceans*, 281, 200-206
- 704 Gneiting, T., & Katzfuss, M. (2014). Probabilistic forecasting. *Annual Review of Statistics and Its*
705 *Application*, 1, 125-151.
- 706 Guan, W., He, X., Pan, D., Gong, F. (2005). Remote sensing estimation of primary productivity in the
707 Bohai Sea, Yellow Sea, and East China Sea. *Journal of Fisheries of China*, 29(3), 367-372.
- 708 Hersbach, H. (2000). Decomposition of the continuous ranked probability score for ensemble
709 prediction systems. *Weather and Forecasting*, 15(5), 559-570.
- 710 Juban, J., Siebert, N., & Kariniotakis, G. N. (2007). Probabilistic short-term wind power forecasting for
711 the optimal management of wind generation. In 2007 IEEE Lausanne Power Tech (pp. 683-688).
712 IEEE.
- 713 Lee, Z., Marra, J., Perry, M. J., Kahru, M. (2015). Estimating Oceanic Primary Productivity from
714 Ocean Color Remote Sensing: A Strategic Assessment. *Journal of Marine Systems*, 149, 50-59.
- 715 Li, W., Tiwari, S. P., El-Askary, H. M., Qurban, et al. (2020). Synergistic use of remote sensing and
716 modeling for estimating net primary productivity in the red Sea with VGPM, eppley-VGPM, and
717 CbPM models intercomparison. *IEEE Transactions on Geoscience and Remote Sensing*, 58(12),
718 8717-8734.
- 719 Matheson, J. E., & Winkler, R. L. (1976). Scoring rules for continuous probability
720 distributions. *Management science*, 22(10), 1087-1096.
- 721 Milutinović, S., & Bertino, L. (2011). Assessment and propagation of uncertainties in input terms
722 through an ocean-color-based model of primary productivity. *Remote Sensing of*
723 *Environment*, 115(8), 1906-1917.
- 724 Pan, X., Wong, G. T., Shiah, F. K., & Ho, T. Y. (2012). Enhancement of biological productivity by
725 internal waves: observations in the summertime in the northern South China Sea. *Journal of*
726 *oceanography*, 68, 427-437.
- 727 Pic, R., Dombry, C., Naveau, P., & Taillardat, M. (2023). Distributional regression and its evaluation
728 with the CRPS: Bounds and convergence of the minimax risk. *International Journal of*
729 *Forecasting*, 39(4), 1564-1572.
- 730 Platt, T., & Sathyendranath, S. (1988). Oceanic primary production: estimation by remote sensing at
731 local and regional scales. *Science*, 241(4873), 1613-1620.
- 732 Platt, T., Caverhill, C., & Sathyendranath, S. (1991). Basin-scale estimates of oceanic primary
733 production by remote sensing: The North Atlantic. *Journal of Geophysical Research: Oceans*,
734 96(C8), 15147-15159.
- 735 Ryther, J. H. (1956). Photosynthesis in the Ocean as a Function of Light Intensity I. *Limnology and*
736 *Oceanography*, 1(1), 61-70.
- 737 Ryther, J. H., & Yentsch, C. S. (1957). The estimation of phytoplankton production in the ocean from
738 chlorophyll and light data I. *Limnology and oceanography*, 2(3), 281-286.
- 739 Saba, V. S., Friedrichs, M. A., Antoine, D., Armstrong, R. A., Asanuma, I., Behrenfeld, M. J., ... &



- 740 Westberry, T. K. (2011). An evaluation of ocean color model estimates of marine primary
741 productivity in coastal and pelagic regions across the globe. *Biogeosciences*, 8(2), 489-503.
- 742 Sathyendranath, S., Longhurst, A., Caverhill, C. M., & Platt, T. (1995). Regionally and seasonally
743 differentiated primary production in the North Atlantic. *Deep Sea Research Part I: Oceanographic*
744 *Research Papers*, 42(10), 1773-1802.
- 745 Schepen, A., Zhao, T., Wang, Q. J., & Robertson, D. E. (2018). A Bayesian modelling method for
746 post-processing daily sub-seasonal to seasonal rainfall forecasts from global climate models and
747 evaluation for 12 Australian catchments. *Hydrology and Earth System Sciences*, 22(2),
748 1615-1628.
- 749 Schwanenberg, D., Fan, F. M., Naumann, S., Kuwajima, J. I., Montero, R. A., & Assis dos Reis, A.
750 (2015). Short-term reservoir optimization for flood mitigation under meteorological and
751 hydrological forecast uncertainty. *Water Resources Management*, 29(5), 1635-1651.
- 752 Silsbe, G. M., M. J. Behrenfeld, K. H. Halsey, A. J. Milligan, and T. K. Westberry. (2016), The CAFE
753 model: A net production model for global ocean phytoplankton, *Global Biogeochem. Cycles*, 30,
754 1756–1777, doi:10.1002/2016GB005521.
- 755 Tan, S. C., Shi, G. Y. (2005). Satellite Remote Sensing of Marine Primary Productivity. *Advances in*
756 *Earth Science. Advances in Earth Science*, 20(8).
- 757 Tan, S. C., Shi, G. Y. (2006). Remote sensing study on the primary productivity and its spatiotemporal
758 variation in the Chinese coastal seas. *Acta Geographica Sinica*, 61(11), 1189-1199.
- 759 Westberry, T. K., Silsbe, G. M., & Behrenfeld, M. J. (2023). Gross and net primary production in the
760 global ocean: An ocean color remote sensing perspective. *Earth-Science Reviews*, 104322.
- 761 Perfors A, Tenenbaum J B, Griffiths T L, et al. A tutorial introduction to Bayesian models of cognitive
762 development[J]. *Cognition*, 2011, 120(3): 302-321.
- 763 Westberry, T., Behrenfeld, M. J., Siegel, D. A., & Boss, E. (2008). Carbon-based primary productivity
764 modeling with vertically resolved photoacclimation. *Global Biogeochemical Cycles*, 22(2).
- 765 Westberry, T., Behrenfeld, M. J., Siegel, D. A., Boss, E. (2008). Carbon-based primary productivity
766 modeling with vertically resolved photoacclimation. *Global Biogeochemical Cycles*, 22(2).
- 767 Yang, B. (2021). Seasonal relationship between net primary and net community production in the
768 subtropical gyres: Insights from satellite and Argo profiling float measurements. *Geophysical*
769 *Research Letters*, 48(17), e2021GL093837.
- 770 Yang, B., Fox, J., Behrenfeld, M. J., Boss, E. S., Haëntjens, N., Halsey, K. H., et al. (2021). In situ
771 estimates of net primary production in the western North Atlantic with Argo profiling floats.
772 *Journal of Geophysical Research: Biogeosciences*, 126, e2020JG006116.
- 773 Zamo, M., & Naveau, P. (2018). Estimation of the continuous ranked probability score with limited
774 information and applications to ensemble weather forecasts. *Mathematical Geosciences*, 50(2),
775 209-234.
- 776 Zhao, T., Wang, Q. J., Bennett, J. C., Robertson, D. E., Shao, Q., & Zhao, J. (2015). Quantifying
777 predictive uncertainty of streamflow forecasts based on a Bayesian joint probability
778 model. *Journal of Hydrology*, 528, 329-340.
- 779 Zhao, T., Wang, Q. J., Bennett, J. C., Robertson, D. E., Shao, Q., & Zhao, J. (2015). Quantifying
780 predictive uncertainty of streamflow forecasts based on a Bayesian joint probability
781 model. *Journal of Hydrology*, 528, 329-340.
- 782



783 **Tables**

784 **Table 1.** Summary of Variables and Data Sources.

Variable name	Variable description	Data source
SST	Sea surface temperature (°C)	
Sal	Salinity (‰)	
TH	Height of tide(m)	
AP	Air pressure (hPa)	Weizhou Marine environment
RH	Relative humidity (%)	monitoring station
SV	Sea visibility (km)	
WS	Wind speed (m·s ⁻¹)	
H/10	1/10th significant wave height (m)	
PAR	Photosynthetically active radiation (W·m ⁻²)	https://oceancolor.gsfc.nasa.gov/
SSP	Sea surface precipitation (mm)	https://www.earthdata.nasa.gov/
SH	Sunshine hours (h·d ⁻¹)	https://data.cma.cn/
VGPM NPP	NPP from the VGPM model (mgC m ⁻² ·d ⁻¹)	http://orca.science.oregonstate.edu/npp.visual.php
CbPM NPP	NPP from the CbPM model (mgC m ⁻² ·d ⁻¹)	
CAFE NPP	NPP from the CAFE model (mgC m ⁻² ·d ⁻¹)	

785 **Table 2.** Summary of Missing Variables.

Variable	SV (km)	H/10 (m)	PAR (W·m ⁻²)	SSP (mm)	SH (h·d ⁻¹)
Missing quantity	31	51	828	378	18

786 **Table 3.** Statistics of data pre- and post-interpolation.

	SV (km)		H/10 (m)		PAR (W·m ⁻²)		SSP (mm)		SH (h·d ⁻¹)	
	pre-	post-	pre-	post-	pre-	post-	pre-	post-	pre-	post-
count	4046	4077	4026	4077	3249	4077	3699	4077	4059	4077
mean	15.22	15.23	0.57	0.57	34.92	35.97	4.94	4.85	5.19	5.18
std	10.33	10.30	0.41	0.41	15.64	15.20	16.13	15.61	3.93	3.93



min	0.00	0.00	0.00	0.00	1.20	1.20	0.00	0.00	0.00	0.00
25%	7.00	7.00	0.30	0.30	22.19	24.14	0.00	0.00	0.80	0.80
50%	12.00	12.00	0.50	0.50	36.03	36.87	0.00	0.00	5.60	5.60
75%	25.00	25.00	0.70	0.70	47.58	48.49	1.30	1.50	8.90	8.80
max	50.00	50.00	4.00	4.00	61.13	61.13	280.40	280.40	12.6	12.6

787

Table 4. Parameters of the Neural Network Model

Hyper-parameters		
Layer Sizes	Layer 1	64
	Layer 2	32
	Layer 3	16
	Layer 4	16
	Layer 5	2
	Distribution Layer	Gaussian distribution
Epochs		800
Learning Rate		0.0001
Batch Size		16
optimizer		Adam
loss		Negative log likelihood

788

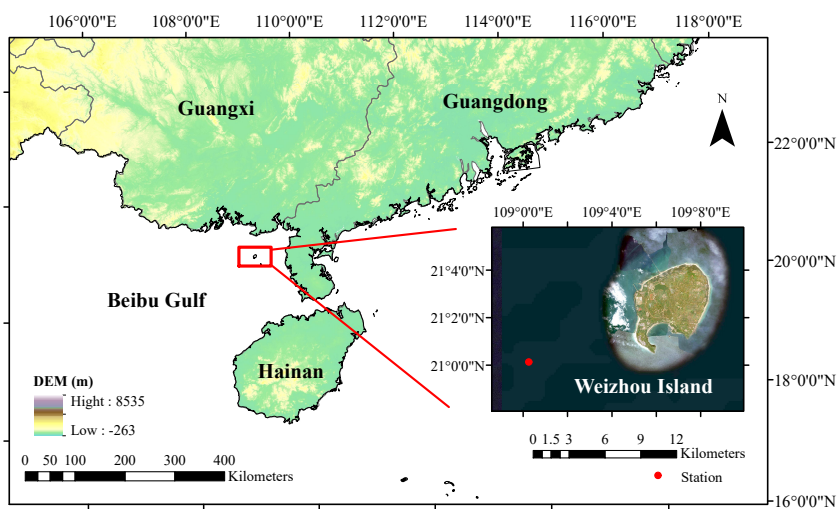
Table 5. CRPS, RMSD, MAPD, and proportion of input data within 95% confidence interval.

	CRPS		RMSD		MAPD		Proportion	
	Train	Test	Train	Test	Train	Test	Train	Test
NN	0.096	0.133	0.149	0.198	11.828	13.237	0.971	0.932
Bayes	0.151	0.20	0.201	0.253	13.909	14.145	0.976	0.951

789

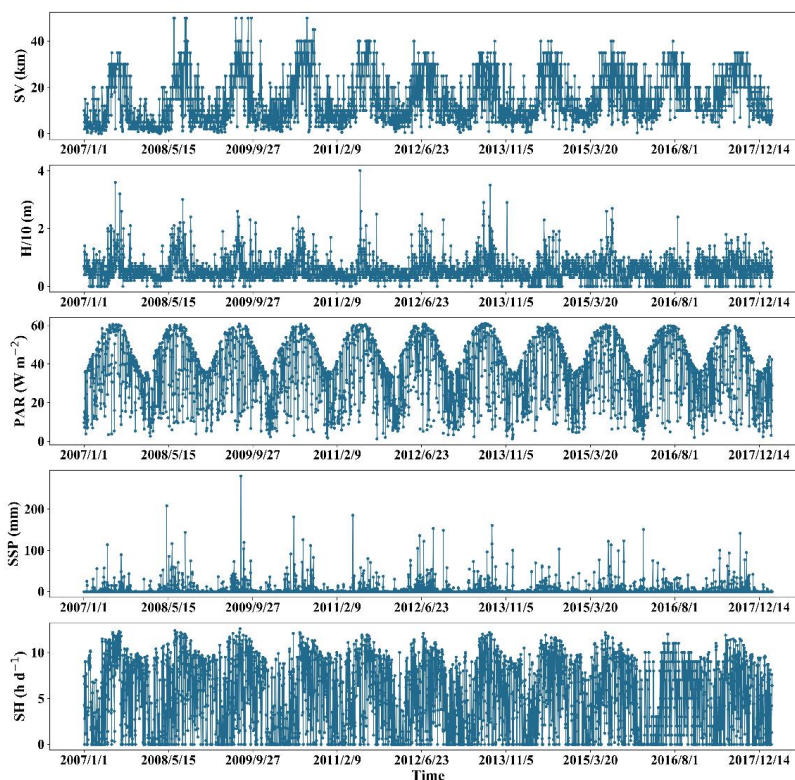


790 **Figures**



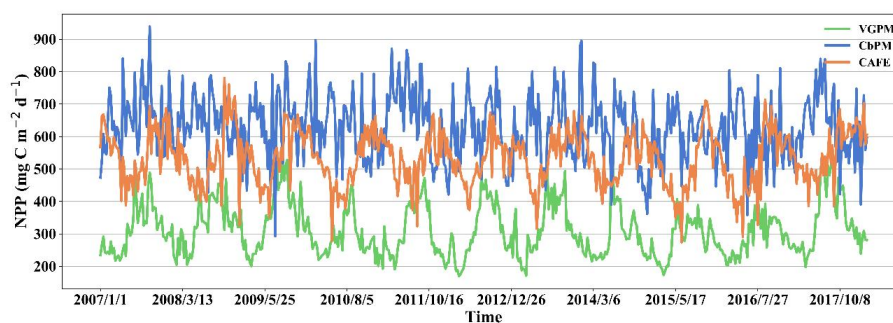
791

792 **Fig. 1.** The research area is located in the waters of Weizhou Island in Beibu Gulf, south China.
793 The red dots in the figure indicate the location of Weizhou Marine Environmental Monitoring
794 Station (21.0017°N, 109.0117°E). Eight distinct sets of monitoring data were collected from this
795 monitoring station.



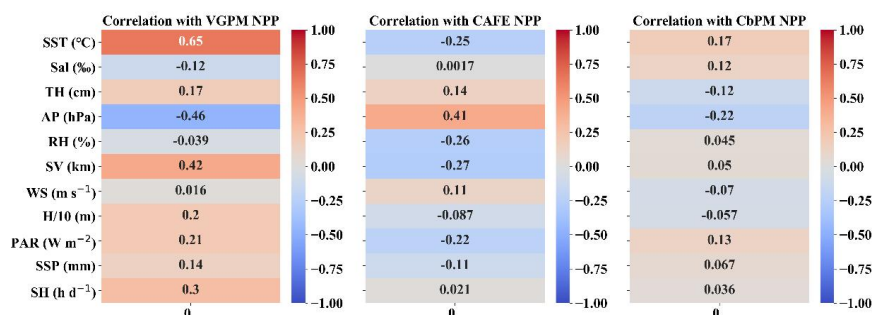
796

797 **Fig. 2.** Time series plots of SV, H/10, PAR, SSP, and SH with missing variables, showing the
798 cyclical variation of these five variables.



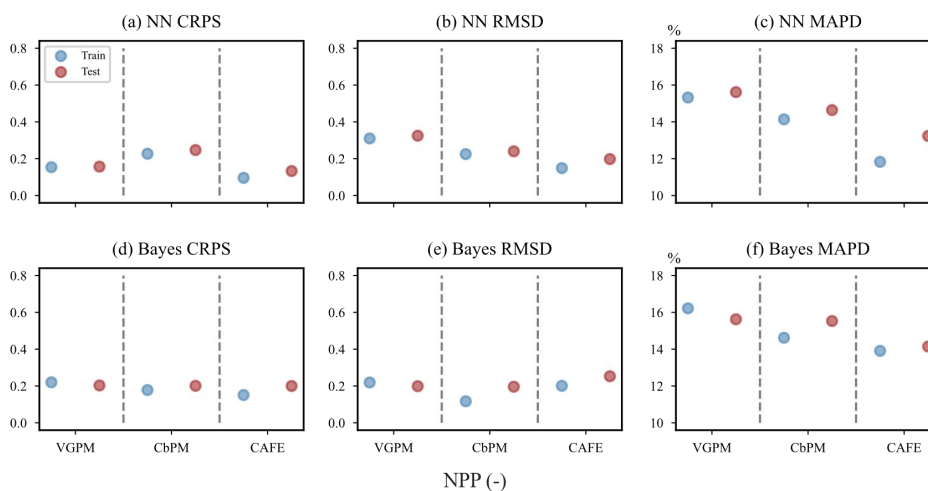
799

800 **Fig. 3.** Time series of VGPM, CbPM, and CAFE NPPs from January 2007 to February 2018,
801 where the green line represents VGPM NPP, the blue line represents CbPM NPP, and the orange
802 line represents CAFE NPP. Abbreviations and data sources can be referenced in Table 1.



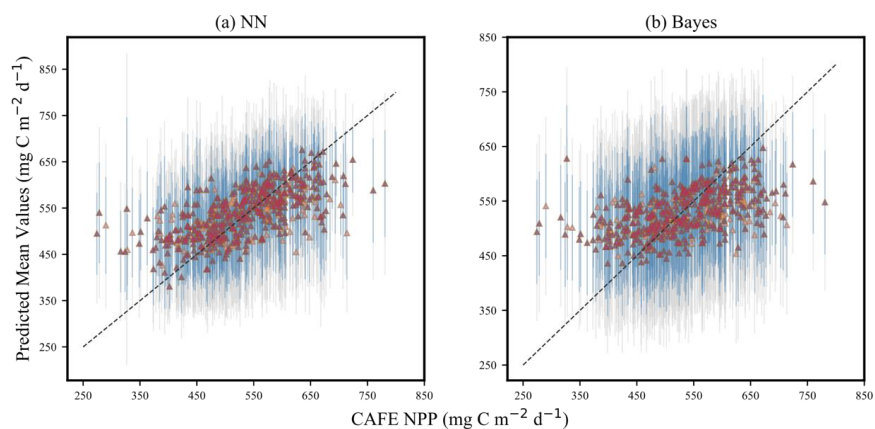
803

804 **Fig. 4.** Pearson correlation of VGPM, CAFE, and CbPM NPPs with input variables. The deeper
 805 the shade of red indicates a stronger positive correlation, whereas the deeper shade of blue
 806 indicates a stronger negative correlation.



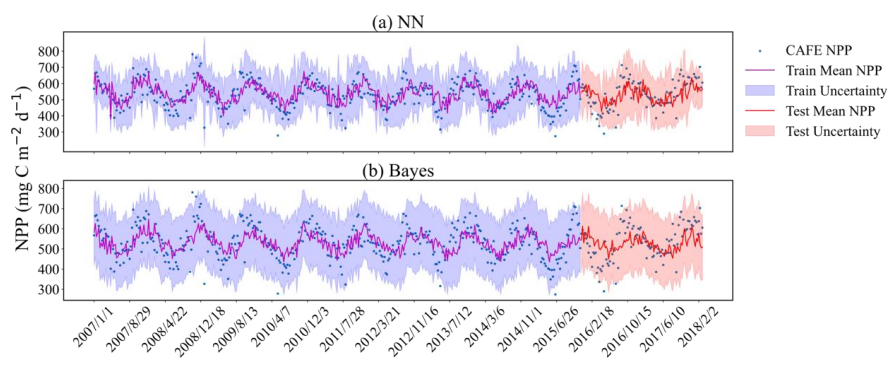
807

808 **Fig. 5.** Comparison of NPP predictive effects from VGPM, CbPM, and CAFE. Panels (a)–(c)
 809 present the results from the neural network-based probabilistic prediction models; panels (d)–(f)
 810 the results from Bayesian probabilistic prediction models based on empirical distributions. The
 811 horizontal coordinates represent the VGPM, CbPM, CAFE NPPs as inputs in sequence, separated
 812 by gray dashed lines, where blue dots represent data from the training set, and red dots denote data
 813 from the test set, and the vertical coordinates are the values of the three metrics, CRPS, RMSD,
 814 MAPD. Since NPP values were normalized to the range of 0 – 1, the y axes of subplots (a), (b),
 815 (d), and (e) are dimensionless. The units for MAPD are percentile.



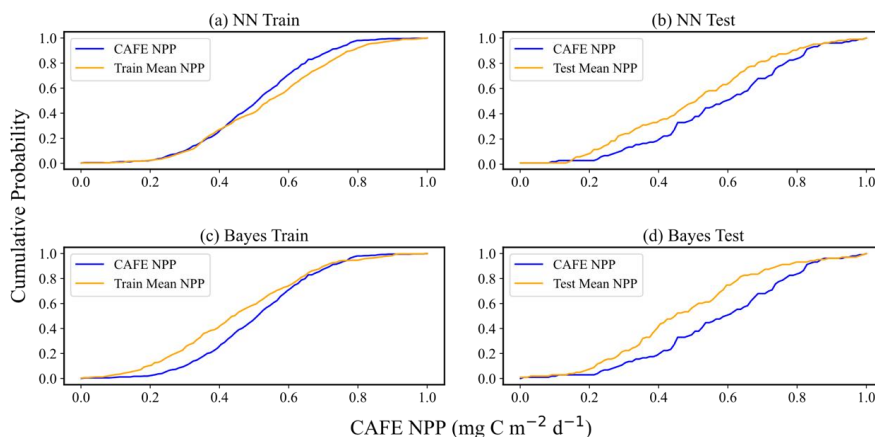
816

817 **Fig. 6.** Uncertainty quantification of (a) neural network-based probabilistic prediction model and
 818 (b) empirical distribution-based Bayesian probabilistic prediction model. The horizontal axes
 819 represent the input VGPM NPP value, while the vertical axes show the mean predicted by the
 820 model. The triangular icons in the figure represent 514 sets of the forecast average, the gray
 821 vertical lines represent the 95% confidence intervals for the predictions, and the blue vertical lines
 822 represent the 75% confidence intervals.



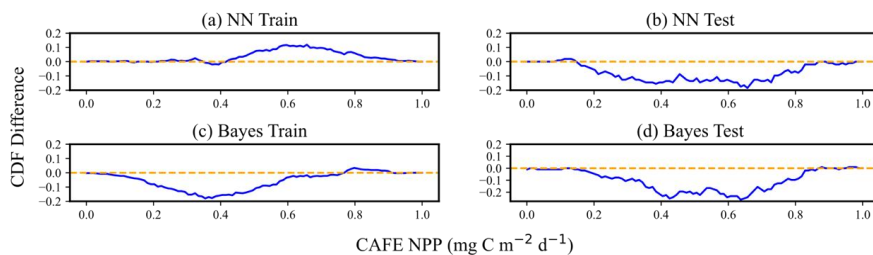
823

824 **Fig. 7.** Comparison of original and predicted mean values shown at an 8-day temporal resolution
 825 within a 95% confidence interval. (a) Probabilistic prediction results based on neural networks; (b)
 826 Bayesian probabilistic prediction results based on empirical distributions. The dashed lines
 827 represent the mean values of the probabilistic predictions. The purple and red shaded areas
 828 illustrate the uncertainty ranges for the training and the test sets, respectively. Blue dots signify
 829 observed data points. All predictions and observations are presented in chronological sequence.



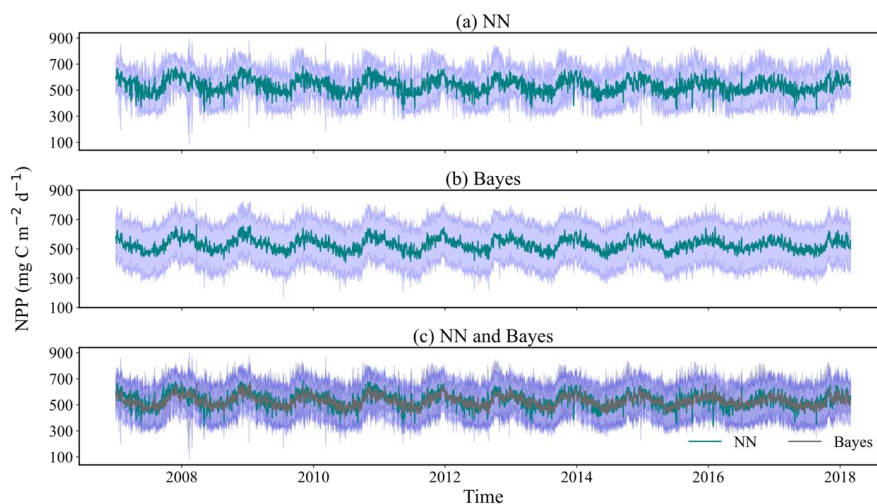
830

831 **Fig. 8.** Comparison of VGPM NPP and predicted mean CDF. Panels (a) and (b) display the
 832 performance of the training and test sets, respectively, in the neural network-based probabilistic
 833 prediction model. Panels (c) and (d) illustrate the performance of the training and test sets,
 834 respectively, in the empirical distribution-based Bayesian probabilistic prediction model. In each
 835 panel, the blue curves represent the CDFs of the VGPM NPP values, while the yellow curves
 836 depict the CDFs of the model's predicted mean values.



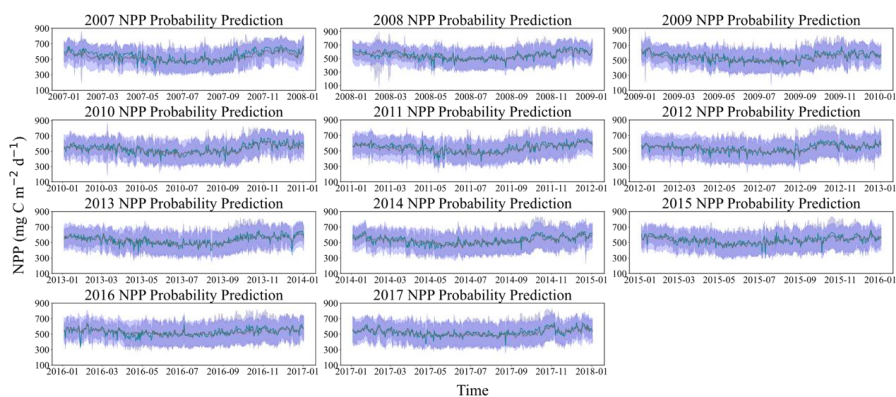
837

838 **Fig. 9.** Difference between the input data CDF and mean CDF of model predictions. Panels (a)
 839 and (b) represent the performance of the training set and test sets, respectively, in the neural
 840 network-based probabilistic prediction model. Panels (c) and (d) showcase the performances of
 841 the training set and test sets, respectively, in the empirical distribution-based Bayesian
 842 probabilistic prediction model. The blue curves in each panel indicate the differential magnitude
 843 of the CDFs. Instances where the blue curves align with the yellow lines denote zero discrepancy
 844 between the input data CDF and the model's predicted mean CDF.



845

846 **Fig. 10.** Time series plots of daily probabilistic NPP predictions in Weizhou Island (2007 – March
847 2018). (a) Probability prediction results of the neural network model; (b) Bayesian probability
848 prediction results based on empirical distribution; (c) Comparison of the two models' predictions,
849 with the green lines representing the mean predictions from the neural network model and the gray
850 lines depicting the mean predictions from the Bayesian model.



851

852 **Fig. 11.** Time series plots of probabilistic NPP predictions in Weizhou Island (2007 – 2017). The
853 light purple shading indicates the 95% confidence interval of the Bayesian model, while the dark
854 purple shading represents the 95% confidence interval of the neural network model. The green
855 lines show the mean prediction values from the neural network model; and the gray lines depict
856 the mean prediction values from the Bayesian model.